This article has been accepted for publication in a future issue of this journal, but has not been fully edited. Content may change prior to final publication. Citation information: DOI 10.1109/TPEL.2017.2683262, IEEE Transactions on Power Electronics

Bipolar Operation Investigation of Current Source Converter-Based Wind Energy Conversion Systems

Qiang Wei, Bin Wu, *Fellow, IEEE*, Dewei (David) Xu, *Member, IEEE*, and Navid R. Zargari, *Fellow, IEEE*

***Abstract*—A series-connected current source converter (CSC)-based configuration has recently been proposed for offshore wind energy conversion systems. A big challenge exists for such a system that its maximum insulation level is the full transmission voltage due to its monopolar operation. This introduces significant burden to the system in terms of cost, reliability, and flexibility. To solve this issue, a bipolar operation giving a half insulation requirement is proposed and investigated in the present work. However, a unique challenge exists for the CSC-based system when operating under bipolar mode, that is the dc-link current control. There are two equivalent paths for the dc-link current which introduces a concern for proper operation of the bipolar system. Accordingly, an optimized dc-link current control is developed in this study. In summary, the bipolar system with the help of the optimized dc-link current control features lower insulation requirement, higher reliability, higher efficiency, and higher flexibility. Finally, both simulation and experimental results are provided.**

***Index Terms*— Current source converter, dc-link current control, efficiency, insulation level, offshore wind energy conversion system.**

I. INTRODUCTION

OFFSHORE wind power is seeing an increased trend because of considerable wind resources, higher and steadier wind speed, and minimized environmental effect [1]. Two main types of configurations are proposed and implemented practically for offshore wind energy conversion systems [2]-[5]: parallel-connected configuration and series-connected configuration. The former is already implemented in practice where the biggest challenge is the very costly and bulky offshore substation required to house step-up transformers, converters, and other related components [6]. The latter is gaining more attention in the literature as the offshore substation can be eliminated, though it has not been implemented yet [6-7].

Apart from voltage source converter (VSC)-based configurations [3-4], [8-10], a couple of current source converter (CSC)-based configurations have also been studied in literature. Compared with thyristor-based configurations [11-12] which feature large footprint, dependent active and reactive power control, and susceptibility to ac network disturbance, the PWM CSC-based ones [13-14] features natural advantages such as simple structure, grid-friendly waveforms, controllable power factor, and reliable grid short-circuit protection. Ref. [13] proposed a series-connected configuration where PWM CSCs are installed on both generator and grid sides, while in [14] the generator-side PWM CSC is replaced with a modular medium-frequency transformer (MFT)-based converter. Compared with the configuration in [13], the one in [14] features smaller size and weight.

One common thing for existing CSC-based series-connected configurations [13-14] is they are all operating under monopolar mode leading significant challenge for system insulation. The wind generator that is farthest from the grounding point must be capable of withstanding a full transmission level which is impractical. To tackle this issue, a three-phase low-frequency high-power transformer is normally connected between the generator and the front-end converter [13]. This transformer, however, is heavy and bulky increasing burden on offshore construction because of the limited space either in the nacelle or in the tower of the wind turbine [7]. On the other hand, a modular medium-frequency transformer (MFT)-based solution is proposed in [14]. Compared with the low-frequency transformer in [13], the modular MFT gives smaller size and weight that is particularly important for offshore construction.

However, the maximum insulation requirement of the system under monopolar operation is still the full transmission level. This introduces significant challenges to the system in terms of cost, reliability, and flexibility.

With a special focus on reducing the maximum insulation level, the present work proposes and investigates a bipolar system. Bipolar mode that typically used in VSCs gives a half insulation requirement compared with monopolar mode. However, a big concern exists for the CSC-based system operating under bipolar mode, that is the dc-link current control. Unlike monopolar mode where there is only one equivalent current path, the bipolar operation mode has two equivalent current paths. Thus, an optimal dc-link current control is required to ensure all the control objectives and give higher efficiency, reliability, and flexibility to the system. Accordingly, an optimized dc-link current control is developed in this study. In summary, the bipolar CSC-based

Qiang Wei, Bin Wu, and David Xu are with the Department of Electrical and Computer Engineering, Ryerson University, 350 Victoria St, Toronto, ON, M5B 2K3, Canada (e-mail: qiang.wei@ryerson.ca; bwu@ee.ryerson.ca; dxu@ryerson.ca).

Navid Reza Zargari is with the Medium Voltage R&D Department, Rockwell Automation Canada, Cambridge, ON N1R5X1, Canada (e-mail: nrzargari@ra.rockwell.com).

This article has been accepted for publication in a future issue of this journal, but has not been fully edited. Content may change prior to final publication. Citation information: DOI 10.1109/TPEL.2017.2683262, IEEE Transactions on Power Electronics

series-connected configuration with the help of the optimized dc-link current control features lower insulation requirement, higher efficiency, reliability, and flexibility.

II. PWM CSC-Based Wind Energy Conversion System

Fig. 1 shows the recently proposed PWM CSC-based configuration for offshore wind farms. In the offshore part, a number of medium-voltage (MV) permanent magnet synchronous generator (PMSG)-based wind generation units are connected in series to reach a high-voltage direct current (HVDC) level. A modular MFT-based converter with a series-input and series-output structure is used interfacing each generator. In the onshore part, a number of MV CSCs are connected in series to form a dc/ac converter. The step-up multi-winding transformers are employed to connect the converters to the grid, providing isolation and grid integration. A dc-link inductor, that is L_{dc}, is shared by offshore and onshore converters.

The overall control scheme of the PWM CSC-based wind farm consists of two parts. One is the control scheme for offshore converters. The other is the control for onshore converters. The onshore control objectives include the maximum power point tracking (MPPT) and voltage balancing control, while the dc-link current control and reactive power control are implemented on the onshore converters. It is worth noting that the dc-link reference current determination shown in Fig. 1 plays a crucial role in the control system which will be thoroughly presented in the following section. Please refer to [14] for more details.

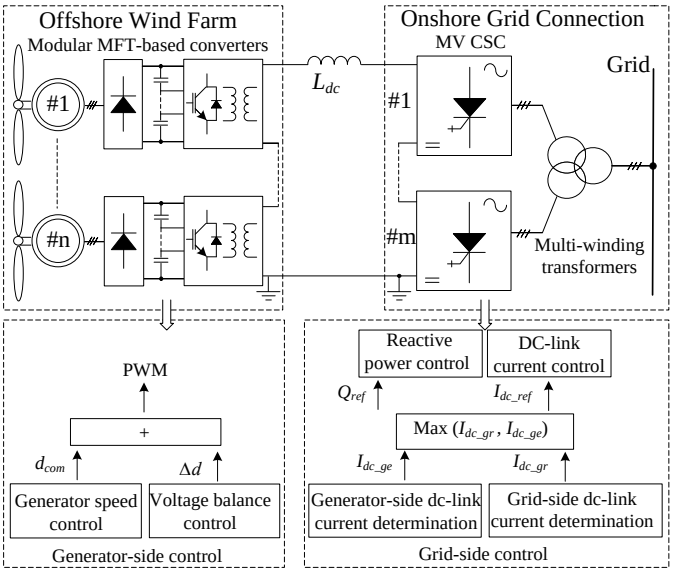

Fig. 1. PWM CSC-based offshore wind farm [14].

In such a series-connected CSC-based system shown in Fig. 1, the generator insulation should be carefully considered. The wind generator that is farthest from the grounding point must be capable of withstanding full transmission voltage which is impractical. To tackle this issue, a couple of methods are developed as follows [15-16]:

(a) insulate the generator winding, and offshore converter for high potential (the full transmission voltage) to the ground, or
(b) insulate the wind turbine tower for high potential (the full transmission voltage) to the ground and keep the nacelle on high potential, or
(c) using transformers.

Among all these methods, the transformer-based one is more reasonable in practice. Ref [13] employed a low-frequency high-power transformer connected between the generator and the generator-side converter that a generator with regular insulation level can be used. This low-frequency transformer is heavy and bulky that increases burden on offshore construction because of the limited space either in the nacelle or in the tower of the wind turbine [7]. To solve this issue, a modular MFTs-based solution is proposed recently [14]. And it is smaller in size and weight compared with the one in [13].

However, there is still a big challenge for the modular MFTs-based system shown in Fig. 1, that is the high insulation level. The maximum insulation level is the full transmission voltage under monopolar mode. A couple of disadvantages associated with such a high insulation requirement exist. First, the high cost on insulation is significant. Compared with its VSC counterpart where the maximum insulation is half of the transmission voltage, the cost on the full transmission-level insulation is higher. Second, the reliability is reduced. The system reliability is decreased as an increased high-voltage isolation requirement. Third, the power transferring capacity is limited. More modules have to be connected in series to reach a higher power capacity, which is impractical beyond certain power ratings mainly due to the limitation of the increased insulation requirement. Fourth, the implementation of the modular MFTs is increasingly challenging as increased insulation requirement as the technology of the high-power modular MFTs with an HVDC-level insulation requirement, 300 kV and higher, for example, is immature [17]. To sum up, the monopolar system with a full transmission-level insulation requirement lower the performance of the system in terms of cost, reliability, power capacity, and implementation feasibility. In turn, a lower insulation requirement will benefit the system in the same way.

Therefore, a bipolar system is proposed and investigated in this study shown in Fig. 2. Bipolar mode normally used in VSCs gives a half insulation requirement compared with monopolar mode, thus, the system performance as mentioned above will be highly enhanced. However, there is a big concern when operating the CSC-based system under bipolar mode. Unlike monopolar mode where there is only one equivalent current path, the bipolar mode has two equivalent current paths shown in Fig. 2. Then, the dc-link current control will be a challenge as (1) all the control objectives achieved in monopolar mode should be ensured under bipolar mode; and (2) the efficiency and flexibility of the system cannot be affected. Accordingly, an optimized dc-link current control is developed and will be discussed in detail in the following section.

This article has been accepted for publication in a future issue of this journal, but has not been fully edited. Content may change prior to final publication. Citation information: DOI 10.1109/TPEL.2017.2683262, IEEE Transactions on Power Electronics

III. Optimized DC-Link Current Control

The dc-link current plays the most critical role in the CSC-based wind farm. Two constraints are normally set for the dc-link current control [13-14]. First, the dc-link reference current should be equal or greater that the maximum value between generator- and grid-side determined minimum dc-link reference currents. Otherwise, the generator-side control objectives, such as MPPT, and the grid-side control objectives, such as unity power factor (UPF), cannot be achieved simultaneously. Second, the dc-link current should be kept as small as possible to lower operation losses. Unlike a VSC-based wind farm where the dc-link voltage is controlled at a constant value, the dc-link current in a CSC-based wind farm can either be constant or varied according to the variation in the input power. The fixed dc-link current operation gives a faster dynamic response but at the expense of higher system losses during low wind speeds [1], while a variable dc-link current significantly reduces the system losses during low wind speed with the penalty of low dynamic performance [1]. A faster dynamic response, however, is not required in wind energy system because the large inertia of the turbine-generator system gives slow change in the output power. On the other hand, a high efficiency is much more preferred for a wind farm.

Considering the wind farm with a series-connected structure under monopolar mode shown in Fig. 1, the dc-link current through all converters has to be same. However, the wind speed at each turbine cannot be guaranteed to be identical. The inconsistency of wind speed leads to different minimum dc-link reference currents for each turbine unit according to its generated power. This will address a considerable challenge for the system operation. To ensure all control objectives, the maximum value among all these minimum reference currents is selected to be the final dc-link reference current of the wind farm [13-14].

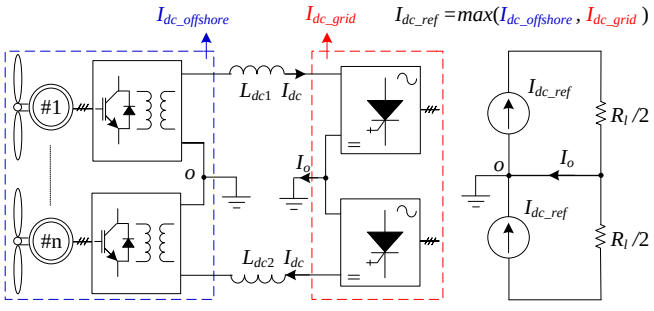

Fig. 2. Bipolar system and its equivalent circuit under conventional dc-link current control.

Following the operation principle in monopolar mode, the equivalent circuit of the bipolar system is derived as shown in Fig. 2. $I_{dc\_offshore}$ is the maximum current among all offshore generator-side minimum reference currents, while I_{dc_grid} is the minimum reference current determined by the onshore CSCs. The larger one is selected to be the final dc-link reference current of the wind farm I_{dc_ref}. Ideally, the current on the earth path (I_o) is zero. R_l denotes the equivalent load of the system. Such a dc-link reference current determination can ensure all the control objectives of the wind farm, but with a penalty of high operation losses which will be thoroughly discussed later.

A. Minimum DC-Link Current by Offshore Converter

The primary objective for the generator-side converter is to obtain MPPT from varying wind speeds. This can be achieved by regulating the modular MFT-based converter as shown in Fig. 1. A simplified circuit diagram of the offshore converter interfacing the generator unit #n is shown in Fig. 3. The PMSG is simplified with a voltage source (e_s) with a finite source inductance (L_s), representing the back-EMF and the synchronous inductance, respectively. The modular MFT-based converter is simplified with a Buck converter [14]. The load at the dc link is replaced by a current source.

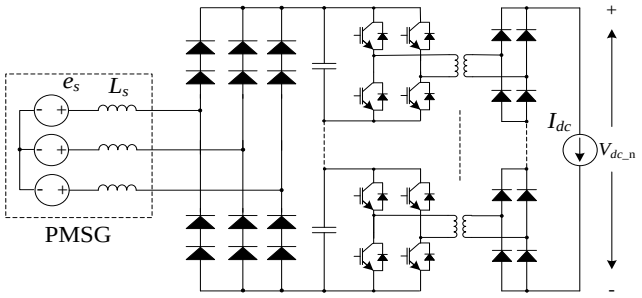

Fig. 3. A simplified modular MFT-based converter for turbine unit #n [14].

Considering the presence of a large input line inductance L_s, the average dc output voltage V_{dc_n} and commutation angle δ can be calculated as follows [18].

$$V_{dc\_n} = \frac{3\sqrt{2}}{\pi} E_{s,LL} - \frac{3}{\pi}\omega_s L_s I_{dc} \tag{1}$$

$$\cos(\delta) = 1 - \frac{\sqrt{2}\omega_s L_s I_{dc}}{E_{s,LL}} \left(0 \le \delta \le 60^\circ\right) \tag{2}$$

where $E_{s,LL}$ is the *rms* value of the line-to-line back-EMF e_s; ω_s is the optimum electrical speed of the PMSG based on MPPT.

It can be observed from (1) and (2) that the longer time the commutation takes the more voltage drops the dc output will suffer. If the commutation angle increases and exceeds 60º, the decrease of the dc voltage will be more rapid until it drops to zero. Rectifier input power factor will decrease as well and the generator stator winding current will increase substantially. This mode of operation is unreasonable and should be avoided.

Assume the captured wind power P_{ge_n} of turbine unit #n that is proportional to the cube of its wind speed (v_w) is transferred to the dc side P_{dc_n} with the loss being neglected, there is

$$P_{dc\_n} = V_{dc\_n} I_{dc} = P_{ge\_n} \propto (v_w)^3 \tag{3}$$

Combining (1) and (3) gives,

This article has been accepted for publication in a future issue of this journal, but has not been fully edited. Content may change prior to final publication. Citation information: DOI 10.1109/TPEL.2017.2683262, IEEE Transactions on Power Electronics

$$P_{ge\_n} = (\frac{3\sqrt{2}}{\pi} E_{s,LL} - \frac{3}{\pi}\omega_s L_s I_{dc}) I_{dc} \tag{4}$$

The dc-link current is therefore calculated as follows

$$I_{dc} = \frac{3\sqrt{2}E_{s,LL} \pm \sqrt{18{E_{s,LL}}^2 - 12\pi\omega_s L_s P_{ge\_n}}}{6\omega_s L_s} \tag{5}$$

To achieve MPPT, a real solution of I_{dc} should be found from (5). Accordingly, the following parameter constraint for the synchronous generator needs to be satisfied.

$${E_{s,LL}}^2 \geq \frac{2\pi}{3}\omega_s L_s P_{ge\_n} \tag{6}$$

Based on (5) and (6), two real solutions are found for the dc-link current. The smaller one is selected while the larger one is unreasonable in practice as it cannot satisfy the prerequisite given in (2). In addition, the lost duty cycle of the modular MFT-based converter due to the presence of the transformer leakage inductance should be compensated [14]. Here, the maximum lost duty cycle is set to 0.1.

In summary, the minimum dc-link reference current determined by the generator unit #n is

$$I_{dc\_ge} = \frac{3\sqrt{2}E_{s,LL} - \sqrt{18{E_{s,LL}}^2 - 12\pi\omega_s L_s P_{ge\_n}}}{6\omega_s L_s \cdot 0.9} \tag{7}$$

Fig. 4 shows the minimum dc-link reference current determined by the generator-side converter. First, the curves are given under different magnetic flux, ranging from 0.8 to 1.2 pu. It's reasonable that when the generator terminal voltage drops as the magnetic flux reduces, the dc-link reference current is increasing accordingly in order to obtain the same amount of power in the dc-link. Second, a higher synchronous inductance gives a slightly larger reference current. In practice, the typical number for the synchronous inductance for PMSG is ranging from 0.3-0.6 pu [1].

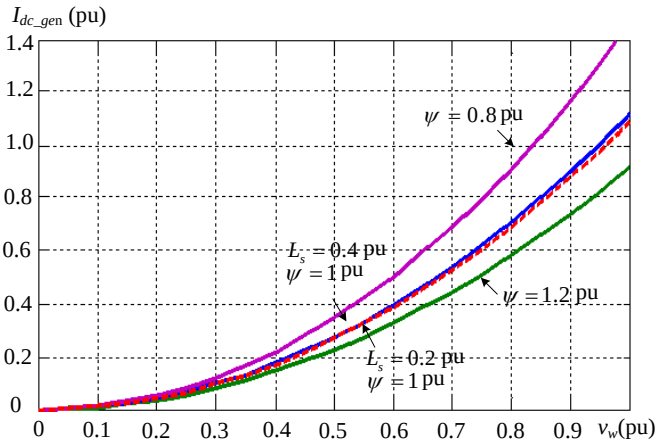

Fig. 4. Reference dc-link current determined by generator-side converter.

B. Minimum DC-Link Current by Onshore Converter

Assuming a lossless system, the captured wind power of turbine unit #n (P_{ge_n}) is equal to the power of the grid-side converter unit #n (P_{gr_n}). Note that in the case of a single turbine system, the reactive power control is normally achieved by the turbine converter itself. In the case of a wind farm, however, it is normally achieved by adding extra reactive support equipment at the plant level, such as STATCOM [19]. Thus, in the present study, only UPF is considered.

With the modulation index m_a of the onshore CSC being set to its maximum value, that is 1, to lower conduction losses [1], and the grid-side resistance R_g being too small that can be neglected, the magnitude of the minimum dc-link current determined by the grid-side converter I_{dc_gr} can be expressed as follows [14]:

$$I_{dc\_gr} = \sqrt{\left\{(1-{\omega_g}^2 L_g C_f)(\frac{2}{3}\frac{P_{gr\_n}}{V_{sd}})\right\}^2 + (\omega_g C_f V_{sd})^2} \tag{8}$$

where w_g is the angular frequency of the grid, C_f is the output filter of the CSC, V_{sd} is the d-axis component of the grid voltage.

C. Final DC-Link Current

The dc-link currents determined by generator- and grid-side converters in the full wind speeds under MPPT and UPF are illustrated in Fig. 5. As mentioned earlier, the larger one is selected to be the final dc-link reference current.

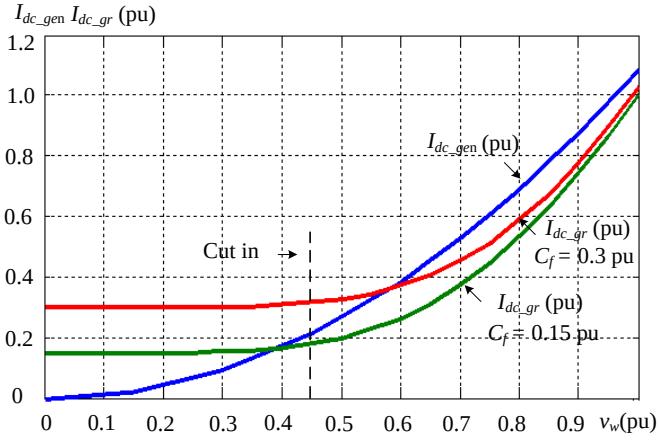

Fig. 5. Reference dc-link current determined by generator- and grid-side converters under MPPT and UPF.

Two conclusions are drawn from Fig. 5. First, a smaller filter capacitor (C_f) requires a lower dc-link reference current. The capacitor at the output of the CSC absorbs considerable amount of leading current. The leading current needs to be compensated when UPF is required by grid codes. In low wind speed ranges (0–0.4pu), the captured real power is very low (the captured wind power is proportional to the cube of the wind speed) and the dc-link current is mainly determined by the reactive current in the capacitors, resulting in almost constant values. As the wind speed goes up, the grid-side dc-link current requirements rise as well as the active current increases. Note

This article has been accepted for publication in a future issue of this journal, but has not been fully edited. Content may change prior to final publication. Citation information: DOI 10.1109/TPEL.2017.2683262, IEEE Transactions on Power Electronics

that the output capacitor filter C_f is normally ranging from 0.15 pu to 0.3 pu for a dual-bridge CSC [20].

Second, the final dc-link reference current of the wind farm is mainly determined by the generator-side converters. For example, in the case of C_f =0.15 pu, the generator-side reference current is higher than that of the grid-side one in the full operation range. A similar result is also found in the case of C_f =0.3 pu, but mainly in high operation ranges, that is ranging from 0.58 to 1 pu.

D. Optimized DC-Link Current Control

On the above basis, an optimized dc-link current control of the bipolar system is proposed. Instead of picking the maximum value among all reference currents to be the final dc-link reference current of the system, two reference currents are selected. One is for the positive link and the other for the negative link of the bipolar system. As a result, the bipolar system is equivalent to two independent monopolar systems with separate dc-link current control. The equivalent circuit is derived as shown in Fig. 6. R_{l_1} and R_{l_2} represent the equivalent loads for upper and lower parts of the bipolar system. I_{dc_ref1} and I_{dc_ref2} are defined as follows.

$$I_{dc\_ref1} = \max(I_{dc\_ge1}, I_{dc\_ge2}, \cdots, I_{dc\_gem}, I_{dc\_gr1}) \tag{9}$$

$$I_{dc\_ref2} = \max(I_{dc\_ge(m+1)}, I_{dc\_ge(m+2)}, \cdots, I_{dc\_gen}, I_{dc\_gr2}) \tag{10}$$

where m is the number of the turbine-generator units with m = n/2. I_{dc_gr1} and I_{dc_gr2} are calculated based on (8).

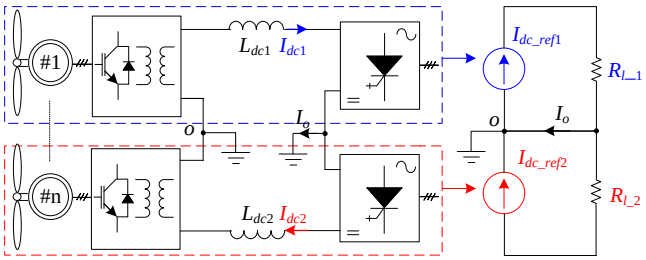

Fig. 6. Optimized dc-link current control.

The optimized dc-link current control ensures all the control objectives achieved in monopolar system. Besides, the overall efficiency and the flexibility of the system are improved.

For simplicity, the operation loss of onshore CSCs is taken as an example. As for a CSC, the switching scheme is that only two switches in the converter are conducted at any instant with one in the top half of the CSC bridge and the other in the bottom half [20]. Therefore, the switching (P_{sw}) and conduction (P_{con}) loss for CSCs can be expressed as follows based on the well-known method [21].

$$P_{sw} = f_{sw}(E_{on}(I_{nom}, V_{nom}) + E_{off}(I_{nom}, V_{nom}))(\frac{i}{I_{nom}})(\frac{v}{V_{nom}}) \tag{11}$$

$$P_{con} = (v_{CE0} + r \cdot i(t)) \cdot i(t) \tag{12}$$

where E_{on} and E_{off} are given in the datasheet of the device, f_{sw} is the switching frequency of the CSC which is normally around 500 Hz, I_{nom} and V_{nom} are the rated current and voltage, while i and v are the instant values during the switching event, v_{CE0} and r are constant values used to calculate the on-state voltage of the device according to its output characteristic provided by the datasheet, and $i(t)$ is the current flowing through the device.

Given a fixed input power, the switching losses of the onshore CSCs for conventional and the proposed scheme are same. This can be verified by (11). The conduction loss of the CSCs is only related to its carrying current as shown in (12). Lower current gives lower conduction losses. Thus, the proposed dc-link current control contributes to lower conduction loss compared with that in conventional scheme shown in Fig. 2.

For example, assuming the maximum wind speed in the upper part of the bipolar system is 1 pu, while it is 0.9 pu for the lower part. the resultant minimum dc-link reference currents are 1.1 pu (I_{dc_ref1}) and 0.88 pu (I_{dc_ref2}) shown in Fig. 6. In the case of conventional dc-link current control, the final dc-link current of the system has to be set to 1.1 pu and flows through both upper and lower parts. In the case of the proposed dc-link current control, the upper and lower parts are controlled independently with their own dc-link currents, 1.1 pu for the upper part, and 0.88 pu for the lower part. Then, the conduction loss under the proposed scheme is reduced to 0.75 pu according to (12) where the base conduction loss is the loss calculated under conventional scheme. As for an MV CSC, the conduction loss of the switches is weighting more than the switching loss, and the typical relationship is around P_{con} = 2.4 P_{sw} [22]. Thus, the total operation loss of the onshore CSCs of the lower part based on the proposed scheme is reduced to 0.82 pu compared with conventional scheme. In addition, a larger mismatch of the maximum wind speed between upper and lower parts contributes to a bigger amount of operation loss saving. For example, the operation loss of the lower part will be reduced to 0.67 pu when the maximum wind speeds for upper and lower parts are 1 pu and 0.8 pu. The same principle also applies to the offshore converters, thus not repeated here.

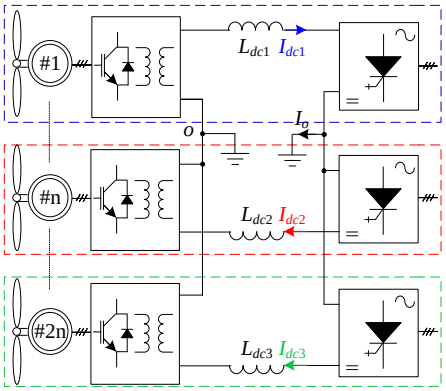

Fig. 7. Multi-terminal system.

Apart from achieving lower operation loss, the proposed dc-link current control gives the bipolar system a higher flexibility. As mentioned earlier, the upper and lower parts of the system are controlled independently. Each part can operate

This article has been accepted for publication in a future issue of this journal, but has not been fully edited. Content may change prior to final publication. Citation information: DOI 10.1109/TPEL.2017.2683262, IEEE Transactions on Power Electronics

on its own dc-link reference current as an independent system with the earth return. Therefore, one part can continue to transmit power in case the other one is out of service for whatever reason (power limitation mode or technical checking). In addition, a large transmission capacity can be achieved by extending the bipolar system to a multi-terminal system as shown in Fig. 7.

IV. Simulation And Experimental Verification

The present focus is the bipolar operation of the CSC-based system with the help of the optimized dc-link current control, while other related objectives such as MPPT, voltage balance control, active and reactive power control, and load current performance (THD, for example) are already thoroughly illustrated in [13-14], [23-25], thus not repeated here. The performance of the bipolar operation has been verified by both Matlab/Simulink simulation and experimental tests. The parameters are listed in Table I.

A. Simulation Results

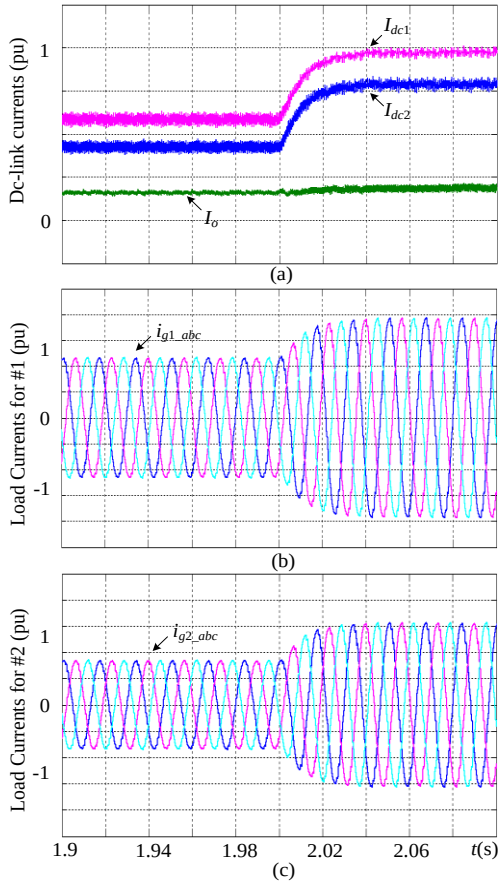

Fig. 8. Simulated performance of the bipolar system under stepped dc-link current.

Fig. 8 illustrates the simulated performance of the bipolar system under stepped dc-link currents. i_{g1_abc} and i_{g2_abc} represent three-phase load currents for Module #1 and #2; I_{dc1} and I_{dc2} are the positive and negative dc-link current of the bipolar system, respectively; I_o is the current on the earth return. Before t = 2s, Module #1 and #2 are operating under steady state that the positive and negative dc-link currents are around I_{dc1} = 0.6 pu, I_{dc2} = 0.44 pu. At t = 2 s, the dc-link reference current for Module #1 is stepped up to 1 pu, while Module # 2 is increasing from 0.44 pu to 0.8 pu on purpose. During this transient period, the dc-link currents, I_{dc1} and I_{dc2}, are well tracking their references. The current on the earth return I_o, is accordingly changed.

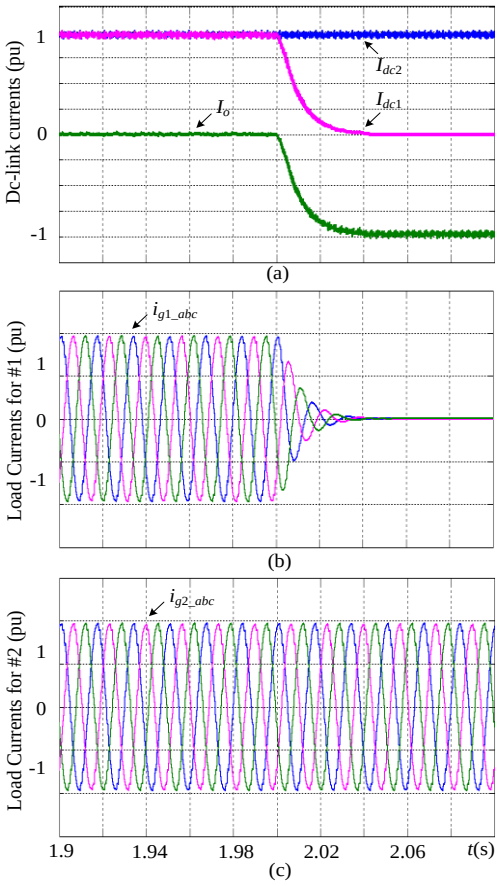

Fig. 9. Simulated performance of the bipolar system when one module is bypassed.

Fig. 9 illustrates the simulated performance of the bipolar system when one module is bypassed. Before t = 2s, Module #1 and #2 are operating under rated condition with $I_{dc1} = I_{dc2}$ = 1 pu. At t = 2 s, the dc-link reference current for Module #1 is set to 0 pu purposely. As a result, the dc-link current and load current for Module #1 are decreasing to 0 pu, while they are maintaining at 1 pu for Module # 2 without any interruption.

B. Experimental Results

A simplified platform is constructed to lower the cost as shown in Fig. 10. Two MFT-based converters and two CSC modules fed with a voltage source are employed to form a lab-scaled bipolar system.

The experimental setup is illustrated in Fig. 11. A dc voltage supply is used to feed the bipolar system. Two MFT-based modules are employed as the front-end converter, and the turn ratios of the three MFTs are set to 1:1 (with a tolerance of ± 2%). Two CSC modules are used to form the dc/ac converter. Each CSC module consists of three integrated modules (SKM300GBD12T4) where a diode is connected in series with an IGBT to function a current source device. A dSPACE DS1103 is used to implement the control algorithms and to

This article has been accepted for publication in a future issue of this journal, but has not been fully edited. Content may change prior to final publication. Citation information: DOI 10.1109/TPEL.2017.2683262, IEEE Transactions on Power Electronics

communicate with the dSPACE control desk of the computer. The modulation schemes used are phase-shifted PWM (MFT-based converter) and SVM (CSC), respectively. As with the simulation, tests under steady and transient states are performed to verify the performance of the bipolar operation.

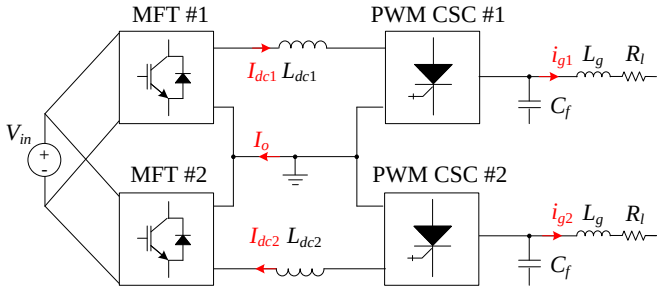

Fig. 10. Simplified circuit for tests.

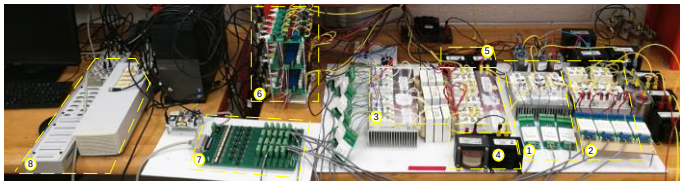

Fig. 11. Experimental setup. (1) CSC Module #1. (2) CSC Module #2. (3) Modular MFT-based converter. (4) Dc-link inductor for Module #2. (5) Dc-link inductor for Module #1. (6) Voltage/current sensor boards. (7) Driver interface board. (8) dSPACE DS1103 processor board.

TABLE I
SIMULATION AND EXPERIMENTAL PARAMETERS

Parameters	Simulation		Experiment	
	SI	pu	SI	pu
System Rating				
Nominal Power	2*1 MW	1.0	2*375 W	1.0
Grid/Load Voltage	4160 V	1.0	60 V	1.0
Rated DC-link Current	195 A	1.0	5 A	1.0
Rated Grid/Load Current	138 A	1.0	3.5 A	1.0
Frequency	60 Hz	1.0	60 Hz	1.0
Generators-Side Converter (MFT-based converter)				
Number of Modules	4		2	
Turn Ratio of Transformers	1:1		1:1	
Switching Frequency	1200 Hz	1.0	1200 Hz	1.0
Grid-Side Converter (CSC)				
Number of Modules	2		2	
DC-link Inductor (L_{dc1}= L_{dc2})	60 mH	1.3	40 mH	1.5
Grid-side inductor	4.59 mH	0.1	5 mH	0.18
Grid-side Capacitor	46 µF	0.3	80 µF	0.3
Switching Frequency	540 Hz	1.0	540 Hz	1.0
Load Resistor	17.3 ohm	1.0	10 ohm	1.0
Modulation Scheme	SVM		SVM	

Fig. 12 shows the experimental performance of the bipolar system under stepped dc-link currents. Before time *t* Module #1 and #2 are operating under steady state with the positive and negative dc-link currents being around I_{dc1} = 0.6 pu (3 A), I_{dc2} = 0.44 pu (2.2 A). At time *t*, the dc-link reference current for Module #1 is set to 1 pu (5 A), while Module # 2 is set to 0.8 pu (4A). Accordingly, the dc-link currents, that are I_{dc1} and I_{dc2}, are tracking their references as shown in Fig. 12. The current through the earth return I_o is changed accordingly. Fig. 13 illustrates the experimental performance of the bipolar system when one module is bypassed. Again, the two modules are operating independently.

It is worth noting that the bipolar system with the help of the optimized dc-link current control is equal to two monopolar systems which are decoupled with each other as analyzed and verified previously. There are two independent dc-link currents, one is for the upper system I_{dc1} (L_{dc1}), and the other for the lower system I_{dc2} (L_{dc2}). Therefore, there is no interaction between the two "independent dc-link current controls" of the equivalent two "independent monopolar systems" of the bipolar system even if $L_{dc1} \neq L_{dc2}$. It is also worth noting that, the situation of $L_{dc1} \neq L_{dc2}$ does not occur (tolerance due to manufacturing technology is excluded). This is because the two equivalent monopolar systems of the bipolar system are with same power rating, thus producing same design in dc-link inductors.

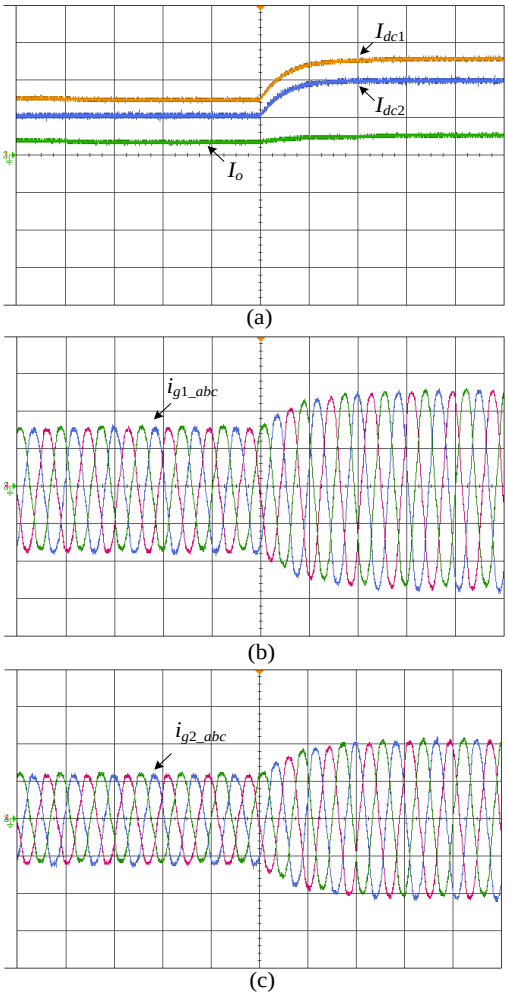

Fig. 12. Experimental performance of the bipolar system under stepped dc-link currents. (a) Dc-link currents and neutral current. I_{dc1}: 2 A/div, I_{dc2}: 2 A/div, I_o: 2 A/div. Time: 20 ms/div. (b) Load currents of Module #1. i_{g1_abc}: 2 A/div. Time: 20 ms/div. (c) Load currents of Module #2. i_{g2_abc}: 2 A/div. Time: 20 ms/div.

This article has been accepted for publication in a future issue of this journal, but has not been fully edited. Content may change prior to final publication. Citation information: DOI 10.1109/TPEL.2017.2683262, IEEE Transactions on Power Electronics

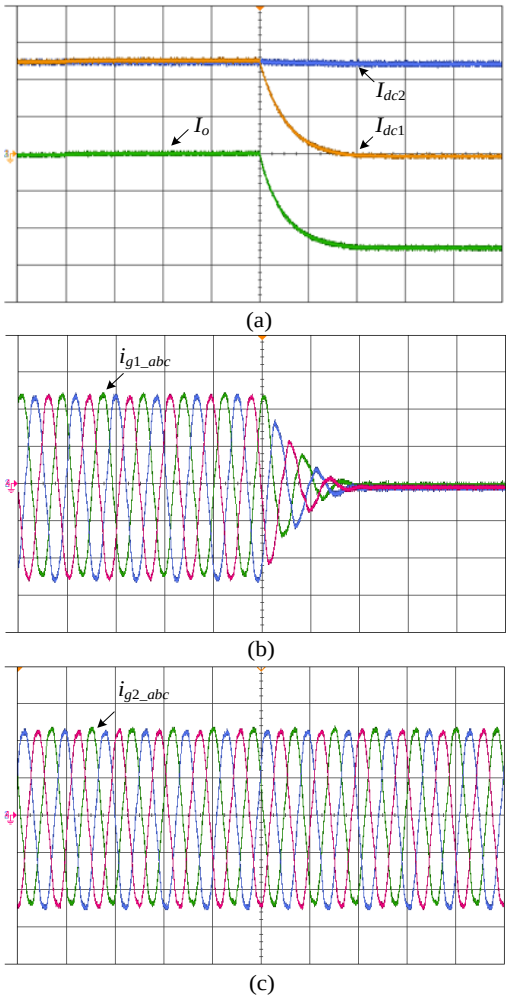

Fig. 13. Experimental performance of the bipolar system when one module is bypassed. (a) Dc-link currents and neutral current. I_{dc1}: 2 A/div, I_{dc2}: 2 A/div, I_o: 2 A/div. Time: 20 ms/div. (b) Load currents of Module #1. i_{g1_abc}: 2 A/div. Time: 20 ms/div. (c) Load currents of Module #2. i_{g2_abc}: 2 A/div. Time: 20 ms/div.

V. Conclusion

In this work, the performance of the CSC-based series-connected offshore wind farm under bipolar operation mode is investigated. Compared with monopolar mode, bipolar mode gives lower insulation level, thus contributing to significant cost saving and higher reliability. In addition, an optimized dc-link current control is developed, based on which the bipolar system is equivalent to two independent monopolar systems that can operate with their own dc-link reference independently with the same earth return. Compared with conventional dc-link current control, the proposed one features higher efficiency and flexibility. Furthermore, the bipolar system can be extended to a multi-terminal system with larger power capacity. In summary, the bipolar system with the help of the optimized dc-link current control features lower insulation level, higher reliability, higher efficiency, and higher flexibility. Both simulation and experimental results are provided in the end.

References

[1] B. Wu, Y. Lang, N. Zargari and S. Kouro, Power Conversion and Control of Wind Energy Systems. Wiley-IEEE Press, 2011.

[2] P. Bresesti, W. Kling, R. Hendriks, and R. Vailati, ‘‘HVDC connection of offshore wind farms to the transmission system,’’ IEEE Trans. Energy Convers., vol. 22, no. 1, pp. 37–43, Mar. 2007.

[3] N. Flourentzou, V. Agelidis, andG. Demetriades, ‘‘VSC-based HVDC power transmission systems: An overview,’’ IEEE Trans. Power Electron., vol. 24, no. 3, pp. 592–602, Mar. 2009.

[4] C. Meyer, M. Hoing, A. Peterson, and R. De Doncker, ‘‘Control and design of DC grids for offshore wind farms,’’ IEEE Trans. Ind. Appl., vol. 43, no. 6, pp. 1475–1482, Nov. 2007.

[5] E. Veilleux and P. Lehn, ‘‘Interconnection of direct-drive wind turbines using a series-connected DC grid,’’ IEEE Trans. Sustain. Energy, vol. 5, no. 1, pp. 139–147, Jan. 2014.

[6] V. Yaramasu, B. Wu, P. C. Sen, S. Kouro and M. Narimani, "High-power wind energy conversion systems: State-of-the-art and emerging technologies," in Proceedings of the IEEE, vol. 103, no. 5, pp. 740-788, May 2015.

[7] Blaabjerg, F.; Ke Ma "Future on Power Electronics for Wind Turbine Systems", Emerging and Selected Topics in Power Electronics, IEEE Journal of, on page(s): 139 - 152 Volume: 1, Issue: 3, Sept. 2013.

[8] Holtsmark, N., Bahirat, H.J., Molinas, M., Mork, B.A., and Hoidalen, H.K. “An All-DC Offshore Wind Farm With Series-Connected Turbines An Alternative to the Classical Parallel AC Model”, IEEE Transactions on Industrial Electronics, vol. 60, no. 6, pp. 2420–2428, Jun. 2012.

[9] S. Lundberg, "Configuration Study of Large Wind Parks", M.S. Thesis, Chalmers Univ. of Technology, Goteborg, Sweden, 2003.

[10] T. H. Nguyen, D. C. Lee and C. K. Kim, "A Series-Connected Topology of a Diode Rectifier and a Voltage-Source Converter for an HVDC Transmission System," IEEE Transactions on Power Electronics, vol. 29, no. 4, pp. 1579-1584, Apr. 2014.

[11] S. Nishikata and F. Tatsuta, “A new interconnecting method for wind turbine/generators in a wind farm and basic performances of the integrated system,” IEEE Transactions on Industrial Electronics, vol. 57, no. 2, pp. 468–475, Feb. 2010.

[12] E. Veilleux and P. Lehn, ‘‘Interconnection of direct-drive wind turbines using a series-connected DC grid,’’ IEEE Transactions on Sustainable Energy, vol. 5, no. 1, pp. 139–147, Jan. 2014.

[13] M. Popat, B.Wu, F.Liu and N. Zargari, “Coordinated control of cascaded current source converter based offshore wind farms,” IEEE Trans. on Sustainable Energy, vol. 3, no. 3, pp. 557-565, 2012.

[14] Q. Wei; B. Wu; D. Xu; N. Zargari, "A Medium Frequency Transformer-Based Wind Energy Conversion System Used for Current Source Converter Based Offshore Wind Farm," IEEE Trans. Power Electron., vol. 32, no. 1, pp. 248-259, Jan. 2017.

[15] D. Jovcic, “Offshore wind farm with a series multiterminal CSI HVDC,” Electro. Power Syst. Res., vol. 78, no. 4, pp. 747–755, Apr. 2008.

[16] S. Lundberg, “Configuration study of large wind parks,” Licentiate thesis, Chalmers Univ. Technol., Dept. of Elect, Power Engg., Goteborg, Sweden, 2003.

[17] E. Agheb and H. Hoidalen, “Medium frequency high power transformers, state of art and challenges,” in Renewable Energy Research and Applications (ICRERA), 2012 International Conference on, 2012, pp. 1–6.

[18] N. Mohan, T. M. Undeland, and W. P. Robbins, Power Electronics: Converters, Applications, and Design: Wiley, 2nd Edition, January 9, 1995.

[19] ABB Statcom. [Online]. Available; http://new.abb.com/facts/statcom, 2017.

[20] B. Wu, High-Power Converters and AC Drives. New York/Piscataway, NJ: Wiley/IEEE Press, 2017.

[21] D. Srajber, W. Lukasch: The calculation of the power dissipation for the IGBT and the inverse diode in circuits with the sinusoidal output voltage; electronica ´92 Proceedings, pp. 51-58.

[22] N. R. Zargari, S. C. Rizzo, Y. Xiao, H. Iwamoto, K. Satoh and J. F. Donlon, "A new current-source converter using a symmetric gate-commutated thyristor (SGCT)," IEEE Transactions on Industry Applications, vol. 37, no. 3, pp. 896-903, May/Jun 2001.

[23] Q. Wei, B. Wu, D. Xu, and N. R. Zargari, “A Natural-Sampling-Based SVM Scheme for Current Source Converter with Superior Low-Order

Harmonics Performance," Power Electronics, Power Electron., vol. 31, no. 9, pp. 6144-6154, Sept. 2016.

[24] Q. Wei, B. Wu, D. D. Xu and N. R. Zargari, "Optimal Space Vector Sequence Investigation Based on Natural Sampling SVM for Medium-Voltage Current-Source Converter," in IEEE Transactions on Power Electronics, vol. 32, no. 1, pp. 176-185, Jan. 2017.

[25] X. Guo, D. Xu, and B. Wu, "Common-mode voltage mitigation for back-to-back current-source converter with optimal space-vector modulation," IEEE Trans. Power Electron., vol. 31, no. 1, pp. 688–697, Jan. 2016.

Qiang Wei received the B.Sc degree from Henan University of Science and Technology, Luoyang, China, in 2008, and the M.A.Sc degree from Xi'an Jiaotong University, Xi'an, China, in 2012 both in electrical engineering, where he is currently working toward the Ph.D. degree in electrical engineering at Ryerson University, Toronto, ON, Canada. From 2012 to 2014, he was with the Delta Power Electronics, Nanjing, China, as an R&D Engineer. His research interests include electric motor drives and renewable energy systems.

Bin Wu (IEEE S'89–M'92–SM'99-F'08) received his M.A.Sc. and Ph.D. degrees in electrical and computer engineering from the University of Toronto, Canada in 1989 and 1993, respectively. He joined Ryerson University in 1993, where he is currently a Professor and Senior NSERC/Rockwell Automation Industrial Research Chair in Power Electronics and Electric Drives. Dr. Wu has published more than 350 technical papers, authored/coauthored two Wiley-IEEE Press books, and holds more than 30 granted/pending US/European patents in the area of power conversion, medium voltage drives, and renewable energy systems. Dr. Wu received the Gold Medal of the Governor General of Canada in 1993, Premier's Research Excellence Award in 2001, NSERC Synergy Award for Innovation in 2002, Ryerson Distinguished Scholar Award in 2003, Ryerson YSGS Outstanding Contribution to Graduate Education Award and Professional Engineers Ontario (PEO) Engineering Excellence Medal in 2014. He is a fellow of Engineering Institute of Canada (EIC) and Canadian Academy of Engineering (CAE).

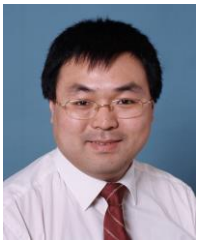

Dewei (David) Xu (S'99–M'01) received the B.Sc, M.A.Sc, and Ph.D. degrees in electrical engineering from Tsinghua University, Beijing, China, respectively in 1996, 1998, and 2001. He has been working in Ryerson University, Toronto, Ontario since 2001, where he is currently Professor. His research interests include renewable energy system, high power converters, electric motor drives and advanced digital control for power electronics.

Navid R. Zargari (IEEE M'94–SM'08–F'15) received the B.Eng. degree from Tehran University, Iran, in 1987 and the M.A.Sc. and Ph.D. degrees from Concordia University, Montreal, Quebec, Canada, in 1991 and 1995 respectively. He has been with Rockwell Automation Canada since November 1994, first as a senior designer, then as the manager of the Medium Voltage R&D department and currently as a Product Architect. For the past 19 years, he has been involved with simulation, analysis, and design of power converters for Medium Voltage AC drives. His research interests include power converter topologies and their control aspects, power semiconductors and renewable energy sources. Dr. Zargari has co-authored more than 80 research papers as well as a book on Power Conversion and Control of Wind Energy Systems. He holds 30 US granted/pending patents in power converters and Medium Voltage applications and was the recipient of the Premier's Award for the Innovator of the year in 2009 from the Province of Ontario.